International Journal of Automotive Technology, Vol. 8, No. 3, pp. 299–308 (2007)

1229-9138/2007/034-06

INTEGRATED CONTROL SYSTEM DESIGN OF ACTIVE FRONT WHEEL STEERING AND FOUR WHEEL TORQUE TO IMPROVE VEHICLE HANDLING AND STABILITY

J. Y. WU*, H. J. TANG, S. Y. LI and S. B. ZHENG

Department of Automation, Shanghai Jiao Tong University, Shanghai 200240, China

(Received 2 November 2006; Revised 29 March 2007)

ABSTRACT–This study proposes a two-layer hierarchical control system that integrates active front wheel steering and four wheel braking torque control to improve vehicle handling performance and stability. The first layer is a robust model matching controller (R-MMC) based on linear matrix inequalities (LMIs), which optimizes an active front steering angle compensation and a desired yaw moment control, and calculates reference wheel slip for the target wheel according to the desired yaw moment. The second layer is a moving sliding mode controller (MSMC) that can track the reference wheel slip in a predetermined time by commanding proper braking torque on the target wheel to achieve the desired yaw moment. Since vehicle sideslip angle measurement is difficult to achieve in practice, a sliding mode observer (SMO) that requires only vehicle yaw rate as the measured input is also developed in this study. The performance and robustness of the SMO and the integrated control system are demonstrated through comprehensive computer simulations. Simulation results reveal the satisfactory tracking ability of the SMO, and the superior improved vehicle handling performance, stability and robustness of the integrated control vehicle.

KEY WORDS : Integrated control system, Robust model matching control, Linear matrix inequality, Moving sliding mode control, Sliding mode observer

NOMENCLATURE

m	: vehicle total mass
m_s	: vehicle sprung mass
h	: height of the sprung mass c.g.
h_s	: distance of the sprung mass c.g. from the roll axes
I_{zz}	: vehicle moment of inertia about yaw axis
I_{xx}	: vehicle moment of inertia about roll axis
I_{xz}	: sprung mass product of inertia
L_f	: distance of c.g. from the front axle
L_r	: distance of c.g. from the rear axle
T_f	: front track width
T_r	: rear track width
C_f	: cornering stiffness of front tire
C_r	: cornering stiffness of rear tire
K_Φ	: roll axis stiffness
D_Φ	: roll axis damping
I_w	: wheel moment of inertia
R_w	: wheel effective rolling radius

*Corresponding author. e-mail: wjylvu@163.com

1. INTRODUCTION

The vehicle active chassis control system has been one of the main areas of research in the automotive industry to improve vehicle safety and handling performance. Active rear steering (ARS) as part of a four wheel steering (4WS) system has been studied extensively and found to enhance vehicle cornering ability by steering the front and rear wheels in accordance vehicle states (Nagai *et al.*, 1991; Qu and Zu, 2005). Nevertheless, the 4WS control system becomes less effective when lateral tire forces approach their adhesion limits and vehicle dynamics show nonlinear characteristics (Horiuchi *et al.*, 1996). Therefore, a direct yaw moment control (DYC) system, with proper distribution of driving or braking torque between the right and left wheels, is proposed to improve vehicle dynamic stability, even if tire lateral forces are approaching their limits (Shino and Nagai, 2001; Boada *et al.*, 2005).

The integrated control system, which properly coordinates four wheel steering and yaw moment control, has the potential to achieve superior vehicle handling performance and stability over 4WS and DYC systems alone (Nagai and Yamanaka, 1996; Mokhiamar and Abe, 2002;

Nohtomi *et al.*, 2005). But this control system has to control the four wheel steering angles, which outweighs the added complexity and cost of the production of such vehicles. Recently, the technology for active front wheel steering integrated with direct yaw moment control is showing a remarkable development (Nagai *et al.*, 2002; Suzumura *et al.*, 2004). In the work of Nagai (2002), a LQ-optimal controller was designed to compensate for the error between the actual state and the desired state of the vehicle. However, the LQ-optimal controller could not guarantee the robustness of the parameter uncertainties and external disturbances (Zhou and Doyle, 1997). Therefore, a two-layer hierarchical control system that integrates active front wheel steering and yaw moment control is presented in this study. This integrated control system has a two-layer hierarchical structure. The first layer is a robust model matching controller (R-MMC) that optimizes an active front wheel steering angle compensation and a desired yaw moment control, and calculates the reference wheel slip for the target wheel according to the desired yaw moment. The calculated reference wheel slip is the input of the second layer, which is a moving sliding mode controller (MSMC) that can track the input accurately and command braking torque on the target wheel to achieve the desired yaw moment. One key feature of the designed integrated control system is that the stability analysis and optimization of the R-MMC are cast in terms of linear matrix inequalities (LMIs). In addition to stability, control considerations such as disturbance rejection, constraints on input and output are also incorporated in the LMIs. The other key feature is that the MSMC traps the system state on the sliding surface at all times, therefore the chattering phenomenon is eliminated and the response speed is improved. In this integrated control system, one of the main assumptions made is the accessibility to vehicle yaw rate and sideslip angle measurement for feedback. The yaw rate can be measured easily using a gyro. But measuring the sideslip angle would represent a disproportional cost in the case of vehicle production (Stéphant *et al.*, 2004). Therefore, a sliding mode observer that requires only the yaw rate as the measured input is also proposed in this study. Simulation results show that the sliding mode observation is highly accurate with respect to the actual sideslip angle, and the integrated control system achieves preferable handling performance and stability. They both maintain good robustness, even if the vehicle parameters and road surface conditions change.

This paper is organized as follows. In section 2, the eight-degree-of-freedom (8-DOF) vehicle and tire models are briefly presented, both including nonlinear characteristics. Section 3 describes the hierarchical integrated control system and the sliding mode observer. The simulation results of the integrated control vehicle are compared with that of a front wheel steering (FWS) vehicle and a DYC only vehicle under slalom maneuver, crosswind disturbance and μ-split road surface conditions in section 4. Finally, Section 5 gives a brief conclusion.

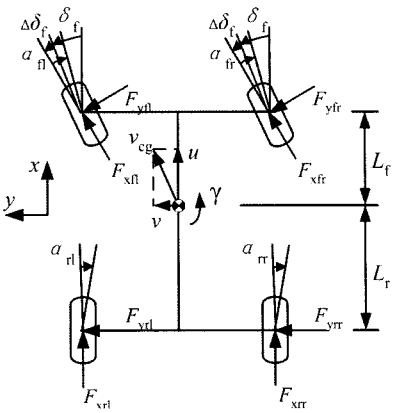

Figure 1. Parameter definitions for the vehicle model.

2. VEHICLE AND TIRE MODELS

2.1. Vehicle Model

The vehicle model used in this study is shown in Figure 1. It is an 8-DOF vehicle model that includes both lateral and longitudinal dynamics as well as the nonlinearities in the system (Kiencke and Nielsen, 2000). Degrees of freedom associated with the model are the longitudinal and lateral velocities, yaw rate, roll rate and four wheel rotational speeds. The dynamics equations governing the motion are derived as:

Longitudinal motion:

$$m(\dot{u} - \gamma v) + m_s h_s \gamma\dot{\phi} = X_{fl} + X_{fr} + X_{rl} + X_{rr}. \quad (1)$$

Lateral motion:

$$m(\dot{v} - \gamma u) + m_s h_s \ddot{\phi} = Y_{fl} + Y_{fr} + Y_{rl} + Y_{rr}. \quad (2)$$

Yaw motion:

$$I_{zz}\dot{\gamma} - I_{xz}\ddot{\phi} = L_f(Y_{fl} + Y_{fr}) - L_r(Y_{rl} + Y_{rr}) - 0.5T_f(X_{fl} - X_{fr}) - 0.5T_r(X_{rl} - X_{rr}). \quad (3)$$

Roll motion:

$$I_{xx}\ddot{\phi} - I_{xz}\dot{\gamma} = m_s h_s(\dot{v} + u\gamma) + m_s h_s g\phi - (K_{\phi f} + K_{\phi r})\phi - (D_{\phi f} + D_{\phi r})\dot{\phi}. \quad (4)$$

Wheel rotational motion:

$$I_w\dot{\omega}_{ij} = -R_w F_{xij} + T_{eij} - T_{bij}. \quad (5)$$

u, v, γ and ϕ are the longitudinal velocity, lateral velocity, yaw rate and vehicle roll angle. F_{xij} and F_{yij} denote the tire longitudinal and lateral forces. The subscripts $i=f, r$ and $j=l, r$ represent the corresponding tire. For example, F_{xfl}

stands for longitudinal tire force on the front left tire. δ_f and δ_r are the front and rear wheel steering angles. α_{ij} represents the wheel slip angle. $\dot{\omega}_{ij}$, T_{eij} and T_{bij} represent the wheel angular acceleration, driving and braking torques. The terms X_{ij} and Y_{ij} are expressed as a function of the longitudinal and lateral tire forces:

$$X_{ij} = F_{xij}\cos\delta_{ij} - F_{yij}\sin\delta_{ij} \tag{6}$$

$$Y_{ij} = F_{xij}\sin\delta_{ij} + F_{yij}\cos\delta_{ij} \tag{7}$$

where ij=*fl*, *fr*, *rl*, *rr*, $\delta_{fl}=\delta_{fr}=\delta_f$ and $\delta_{rl}=\delta_{rr}=\delta_r=0$.

2.2. Tire Model

The modeling of tire force plays an important role in determining the vehicle dynamic behaviors. Generally, the study of the tire model can be categorized into two different approaches. One is the development of the analytical model (Sakai, 1990), the other is the construction of the semi-empirical model (Pacejka, 2002). The latest semi-empirical tire model, Magic Formula by Pacejka, is used in this study for its convenience and accuracy. The general form (sine version) of the formula reads:

$$Y(x)=D\sin\{C\arctan\{Bx-E[Bx-\arctan(Bx)]\}\} \tag{8}$$

where $Y(x)$ is either longitudinal tire force, F_x, with x the longitudinal wheel slip, λ, or lateral tire force, F_y, with x the tire slip angle, α.

Tire self aligning moment, M_z, is calculated as a product of the lateral force and the pneumatic trail, σ_α, which is based on a cosine version of the Magic Formula:

$$Y(x)=D\cos\{C\arctan\{Bx-E[Bx-\arctan(Bx)]\}\} \tag{9}$$

where $Y(x)$ is the pneumatic, σ_α, with x the tire slip angle, α.

The coefficients in the formula depend on the type of tire and road conditions, and its values have been validated with actual tire test data. The forces and moments in the combined slip condition are based on the pure slip characteristics multiplied by a weighting function. The tire model includes the transient behaviors, which means the tire forces and moments should be multiplied by a fist-order lag function.

An important quantity for tire friction force calculation is the wheel vertical load, F_{zij}, which is a function of both the vehicle's static and its dynamic loads transfer. It can be represented as:

$$F_{zfl} = \frac{mgL_r}{2L} - ma_x\frac{h}{2L} - \frac{ma_yL_rh}{LT_f} - \frac{(K_{\phi f}\phi + D_{\phi f}\dot{\phi})}{T_f} \tag{10}$$

$$F_{zfr} = \frac{mgL_r}{2L} - ma_x\frac{h}{2L} + \frac{ma_yL_rh}{LT_f} + \frac{(K_{\phi f}\phi + D_{\phi f}\dot{\phi})}{T_f} \tag{11}$$

$$F_{zrl} = \frac{mgL_f}{2L} + ma_x\frac{h}{2L} - \frac{ma_yL_fh}{LT_r} - \frac{(K_{\phi r}\phi + D_{\phi r}\dot{\phi})}{T_r} \tag{12}$$

$$F_{zrr} = \frac{mgL_f}{2L} + ma_x\frac{h}{2L} + \frac{ma_yL_fh}{LT_r} + \frac{(K_{\phi r}\phi + D_{\phi r}\dot{\phi})}{T_r} \tag{13}$$

where a_x and a_y are the vehicle longitudinal and lateral accelerations.

Tire lateral force calculation depends on the wheel vertical load and slip angle. The slip angle of each wheel is calculated as:

$$\alpha_{fl} = \delta_f - \arctan\left(\frac{v+L_f\gamma}{u-0.5T_f\gamma}\right) + \Delta\delta_f \tag{14}$$

$$\alpha_{fr} = \delta_f - \arctan\left(\frac{v+L_f\gamma}{u+0.5T_f\gamma}\right) + \Delta\delta_f \tag{15}$$

$$\alpha_{rl} = -\arctan\left(\frac{v-L_r\gamma}{u-0.5T_r\gamma}\right) \tag{16}$$

$$\alpha_{rr} = -\arctan\left(\frac{v-L_r\gamma}{u+0.5T_r\gamma}\right). \tag{17}$$

The calculation of wheel longitudinal slip, λ, requires the wheel longitudinal velocity. These wheel longitudinal speeds, taking into account the vehicle lateral dynamics, are calculated as:

$$u_{fl} = \left(u-\frac{T_f}{2}\gamma\right)\cos\delta_f + (v+L_f\gamma)\sin\delta_f \tag{18}$$

$$u_{fr} = \left(u+\frac{T_f}{2}\gamma\right)\cos\delta_f + (v+L_f\gamma)\sin\delta_f \tag{19}$$

$$u_{rl} = u-\frac{T_r}{2}\gamma \tag{20}$$

$$u_{rr} = u+\frac{T_r}{2}\gamma \tag{21}$$

where u_{fl}, u_{fr}, u_{rl} and u_{rr} are the wheel longitudinal velocities for the front left, front right, rear left and rear right wheels respectively. Moreover, the longitudinal wheel slip is defined as:

$$\begin{cases} \lambda_{ij} = \dfrac{R_w\omega_{ij}-u_{ij}}{u_{ij}}, & R_w\omega_{ij} < u_{ij} \\ \lambda_{ij} = \dfrac{R_w\omega_{ij}-u_{ij}}{R_w\omega_{ij}}, & R_w\omega_{ij} \geq u_{ij} \end{cases}. \tag{22}$$

In this paper, the driving torque is not considered, hence the wheel slip is:

$$\lambda_{ij} = \frac{R_w\omega_{ij}-u_{ij}}{u_{ij}}, \quad R_w\omega_{ij} < u_{ij}. \tag{23}$$

3. CONTROL SYSTEM DESIGN

The goal of this control system is to coordinate the active front wheel steering and four wheel braking torque control to improve vehicle maneuverability and stability. Figure 2 shows the block diagram of the control system.

This setup has a hierarchical control structure of two

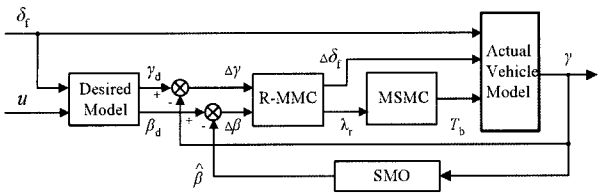

Figure 2. Block diagram of system controller.

layers based on a sliding mode sideslip angle observer. The first layer is an R-MMC controller that optimizes an active front wheel steering angle compensation, $\Delta\delta_f$, and a desired yaw moment control, and calculates the reference wheel slip, λ_r, for the target wheel according to the desired yaw moment. The second layer is an MSMC controller that tracks the calculated reference wheel slip by commanding braking torque, T_b, on the target wheel to achieve the desired yaw moment control. The feedback variable sideslip angle is observed by the SMO.

3.1. Linear Vehicle Model

The bicycle model is a well-known linear approximation of vehicle nonlinear dynamics. To design the control system, this model is described in vehicle co-ordinates, and the lateral motion state space equation is represented as:

$$\dot{x} = Ax + E\delta_f + BU \tag{24}$$

where $x = [\beta \ \gamma]^T$

$$A = \begin{bmatrix} -\dfrac{2(C_f + C_r)}{mu} & -1 - \dfrac{2(L_fC_f - L_rC_r)}{mu^2} \\ -\dfrac{2(L_fC_f - L_rC_r)}{I_{zz}} & -\dfrac{2(L_f^2C_f + L_r^2C_r)}{I_{zz}u} \end{bmatrix},$$

$$E = \begin{bmatrix} \dfrac{2C_f}{mu} \\ \dfrac{2L_fC_f}{I_{zz}} \end{bmatrix}, \quad B = \begin{bmatrix} \dfrac{2C_f}{mu} & 0 \\ \dfrac{2L_fC_f}{I_{zz}} & \dfrac{1}{I_{ZZ}} \end{bmatrix}.$$

β is the sideslip angle. C_f and C_r indicate the cornering stiffness of the front and rear tires.

In the bicycle model, the front and rear wheel slip angles, α_f and α_r, are approximated as:

$$\alpha_f = \delta_f - \beta - \frac{L_f\gamma}{u} + \Delta\delta_f \tag{25}$$

$$\alpha_r = -\beta + \frac{L_r\gamma}{u}. \tag{26}$$

The lateral forces generated by the front and rear tires can be calculated as:

$$F_{yfl} + F_{yfr} \approx -2C_f\alpha_f \tag{27}$$

$$F_{yrl} + F_{yrr} \approx -2C_r\alpha_r. \tag{28}$$

To match the desired model, a control input vector $U=[\Delta\delta_f \ N]$, which includes an active front wheel steering compensation and a desired yaw moment control, is added to the bicycle model. $N=C_\lambda\lambda_{ij}F_{zij}T_i/2$, C_λ is the slope in the linear region of the μ–λ curve and T_i is the track width of the vehicle.

In Figure 2, the desired model generates the reference vehicle dynamic responses corresponding to the driver's steering input. The desired sideslip angle and the desired yaw rate dynamical responses are two independent first-order systems (Shino and Nagai, 2001), and they can be represented as:

$$\begin{cases} \beta_d = \dfrac{k_\beta\delta_f}{1+\tau_\beta S} \\ \gamma_d = \dfrac{u\delta_f}{L(1+u^2/u_{ch}^2)} \cdot \dfrac{1}{1+\tau_r S} \end{cases} \tag{29}$$

where, k_β=0, τ_β is the desired sideslip angle response time constant. $u_{ch}^2 = C_fC_rL^2/m(L_rC_r - L_fC_f)$ is the vehicle characteristic velocity, τ_γ is the desired yaw rate response time constant, and S is the Laplace operator. The module of γ_d should be no larger than $|\mu g/u|$ because the maximum friction coefficient μ is always below 1. The desired vehicle dynamic model can be described by the state space form:

$$\dot{x}_d = A_dx_d + E_d\delta_f = \begin{bmatrix} -\dfrac{1}{\tau_\beta} & 0 \\ 0 & -\dfrac{1}{\tau_r} \end{bmatrix} \begin{bmatrix} \beta_d \\ \gamma_d \end{bmatrix} + \begin{bmatrix} \dfrac{k_\beta}{\tau_\beta} \\ \dfrac{k_r}{\tau_r} \end{bmatrix} \delta_f \tag{30}$$

where $k_r = \dfrac{u}{L(1+u^2/u_{ch}^2)}$. In this study, a desired over steer desired yaw moment control can be obtained by adjusting the slip ratio of the front-outer wheel. Similarly, a desired under steer yaw moment control is obtained by adjusting the slip ratio of the rear-inner wheel. Adjusting wheel slip only one wheel at a time is a simple but effective method. Another advantage of adjusting wheel slip one wheel at a time is that the deceleration of the vehicle is less than it is when adjusting wheel slips of two or more wheels with the same amount of yaw moment generated (Kimbrough, 1999).

3.2. Robust Model Matching Controller Design

In order to make the actual sideslip angle and yaw rate follow their desired values, the error variables are defined as:

$$e = x_d - x = [\Delta\beta \ \Delta\gamma]^T. \tag{31}$$

Accordingly, the error state space equation derived from equation (24) and equation (30) is:

$$\dot{e} = \dot{x}_d - \dot{x} = A_d(x_d - x) + (A_d - A)x + (E_d - E)\delta_f - BU \tag{32}$$

So the augmented error state space equation becomes:

$$\begin{bmatrix} \dot{e} \\ \dot{x} \end{bmatrix} = \begin{bmatrix} A_d & A_d - A \\ 0_{2\times2} & A \end{bmatrix} \begin{bmatrix} x_d - x \\ x \end{bmatrix} + \begin{bmatrix} E_d - E \\ E \end{bmatrix} \delta_f + \begin{bmatrix} -B \\ B \end{bmatrix} U \tag{33}$$

Equation (33) can be further expressed as:

$$\dot{X} = A_1 X + B_1 W + B_2 U \tag{34}$$

where state vector $X = \begin{bmatrix} x_d - x \\ x \end{bmatrix} = [\Delta\beta \ \ \Delta\gamma \ \ \beta \ \ \gamma]^T$, state matrices $A_1 = \begin{bmatrix} A_d & A_d - A \\ 0_{2\times 2} & A \end{bmatrix}$, $B_1 = \begin{bmatrix} E_d - E \\ E \end{bmatrix}$, $B_2 = \begin{bmatrix} -B \\ B \end{bmatrix}$, input disturbance $W=\delta_f$, control input $U=[\Delta\delta_f \ N]^T$.

In this study, we cast the control problem into a multiobjective H_∞ optimal controller design in terms of LMIs. The LMI-based design allows us to systematically design a controller satisfying not only the quadratic stability but also disturbance rejection, constraints on input and output, etc. Then, the performance output vector, Z, is defined as:

$$Z = \left[\Delta\beta \ \ \Delta\gamma \ \ \Delta\delta_f \ \ N\right]^T = C_1 X + D_{11} W + D_{12} U \tag{35}$$

where C_1, D_{11} and D_{12} are state matrices derived from equation (34). The output feedback variables, Y, are defined as:

$$Y = [\Delta\beta \ \ \Delta\gamma]^T = C_2 X + D_{21} W + D_{22} U \tag{36}$$

where C_2, D_{21} and D_{22} are also state matrices derived from equation (34).

Actually, each measurement variable is somewhat 'polluted' by sensor noise or estimation error, therefore the output feedback variables must consider the influence of noise. That is:

$$Y_m = Y + W_n \tag{37}$$

where $W_n=[n_1 \ n_2]^T$ are noises added to the feedback variables. Then the input disturbance vector, W, is augmented as $\overline{W} = \left[\delta_f \ \ n_1 \ \ n_2\right]^T$.

Combining equation (34), equation (35) and equation (37), the state space realization of this error model is:

$$G_p \square \left[\begin{array}{c|cc} A_1 & \overline{B}_1 & B_2 \\ \hline C_1 & \overline{D}_{11} & D_{12} \\ C_2 & \overline{D}_{21} & D_{22} \end{array}\right] \tag{38}$$

where $\overline{B}_1 = [B_1 \ 0_{4\times 2}]$, $\overline{D}_{11} = [D_{11} \ 0_{4\times 2}]$ and $\overline{D}_{21} = [D_{21} \ I_{2\times 2}]$ are the augments of state matrices B_1, D_{11} and D_{21}.

Scaling is very important in model analysis and controller design, and the weighting functions reflect the required performance of the system. To do this, decisions are made on the expected magnitudes of disturbances and each input signal, and on the allowed deviation of performance output (Skogestad and Postlethwaite, 1996). Denoting the input weighting matrix as W_{in} and the output weighting matrix as W_{out}, the system transfer function matrices from input vector $[\overline{W} \ U]^T$ to output vector $[Z \ Y_m]^T$ are:

$$G = W_{out} G_p W_{in}. \tag{39}$$

The essential of H_∞ control is to design a controller, K, such that the resultant close loop system is robustly stable to the worst possible disturbance. The H_∞ normal of the transfer function matrix from input disturbance to performance output satisfies:

$$\left\| T_{Z\overline{W}} \right\|_\infty = \sup_\omega \sigma_{\max}[T_{Z\overline{W}}(j\omega)] \le \zeta \tag{40}$$

where $\sigma_{\max}$ is the maximum singular value of the closed loop transfer function $T_{Z\overline{W}}$, and ζ is the specified close loop performance. The LMI-based H_∞ optimal approach is computationally more involved for large problems, and allows the treatment of uncertain systems by stabilizing several systems simultaneously and immediately. In comparison, the LMI approach has the merit of eliminating the regularity restrictions attached to the Riccati-based solution, and the H_∞ performance is directly optimized by solving the linear matrix inequalities problem (Gahinet *et al.*, 1995).

3.3. Moving Sliding Mode Wheel Slip Controller

By controlling wheel slip, one can control the force generated by the tire. That means we can achieve a yaw moment control by assigning an appropriate wheel slip to the target wheel. Sliding mode control is a popular and effective method for achieving robust tracking of nonlinear systems. In this section, a moving sliding mode controller is designed to track the reference wheel slip input. In contrast to the fixed sliding surface of the conventional sliding mode control, the sliding mode controller in this paper has a moving (time-varying) sliding surface. Therefore, the states lie on the sliding surface all the time. The controller improves the system performance in terms of eliminating the chatting phenomenon, a decrease in the reaching time and robustness to parameter variations (Edwards and Spurgeon, 1998).

Differentiating equation (23) with respect to time gives the derivative form:

$$\dot{\lambda} = \frac{1}{u}\left[R_w \dot{\omega} - \frac{R_w \omega}{u}\dot{u}\right]. \tag{41}$$

Substituting equation (5) and equation (23) into equation (41) yields:

$$\dot{\lambda} = \frac{1}{u}\left[\frac{R_w}{I_w}(-R_w F_x - T_b) - (1+\lambda)\dot{u}\right] = f - \frac{R_w}{uI_w} T_b \tag{42}$$

where $f = -\frac{1}{u}\left[\frac{R_w^2 F_x}{I_w} + (1+\lambda)\dot{u}\right]$. The control object is to drive the system states $(\lambda, \dot{\lambda})$ to the reference values $(\lambda_r, \dot{\lambda}_r)$ by applying wheel braking torque, T_b (assuming $\dot{\lambda}_r = 0$ at all times). Based on the work of Bartoszewicz (1995), Roy and Olgac (1997) and Chun and Sunwoo (2004), the switching function, s, is defined as:

$$s = \lambda - k(t)\lambda_r \tag{43}$$

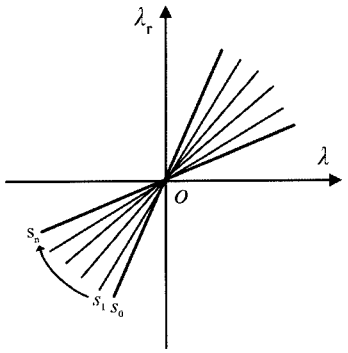

Figure 3. Rotating sliding surface ($\lambda_r < 0$).

where $k(t) = at + b = \frac{1}{t_f}(1 - \frac{\lambda_0}{\lambda_r})t + \frac{\lambda_0}{\lambda_r}$ is the slope of the sliding surface. The time-varying sliding surface slope is designed by using the initial state and the final sliding surface for maintaining the sliding motion from the beginning. The moving sliding surface in equation (43) is shown in Figure 3, where $k_0 = \lambda_0/\lambda_r$ and $k_t \approx 1$. Parameter t_f, which can be predetermined, is related to the response time and the control input.

The control that moves the state $(\lambda, \dot{\lambda})$ along the sliding surface defined by $s=0$ is the equivalent control, $T_{b,eq}$. Differentiating equation (43), we arrive at:

$$\dot{s} = \ddot{\lambda} - a\dot{\lambda}_r \cdot \tag{44}$$

Under the equivalent control braking torque, the sliding motions are governed by $\dot{s}=0$. That is:

$$\ddot{\lambda} = a\dot{\lambda}_r \cdot \tag{45}$$

Substituting equation (42) into equation (45) gives:

$$f - \frac{R_w}{uI_w} T_{b,eq} = a\dot{\lambda}_r . \tag{46}$$

Solving for the equivalent control braking torque, $T_{b,eq}$:

$$T_{b,eq} = \frac{uI_w}{R_w}(f - a\dot{\lambda}_r) \cdot \tag{47}$$

The dynamic value of f, which can not be calculated accurately, is estimated as $\hat{f}$. Neglecting the errors on wheel angular velocity from sensors, the estimation error of f is mainly affected by the estimated longitudinal tire force, $\hat{F}_x$. One benefit using sliding mode control is that it can handle parameter uncertainty as long as one knows the parameter bounds (Khalil, 1996). Here, the estimation error of f is bounded by some known function, F. That is:

$$|f - \hat{f}| \le F \tag{48}$$

where $f - \hat{f} = \frac{R_w^2}{uI_w}(\hat{F}_x - F_x)$. Then the approximate equivalent control braking torque, $\hat{T}_{b,eq}$, is:

$$\hat{T}_{b,eq} = \frac{uI_w}{R_w}(\hat{f} - a\dot{\lambda}_r) . \tag{49}$$

The switching function, s, is used by the sliding mode control to change the structure of the control law. The most common way is to use the sign of the switching function, sin(□). In a real system, disturbance and parameter uncertainty always exist, therefore an additional term called hitting control braking torque, $T_{b,h}$, has to be added to the overall braking torque control. Define the overall braking torque control, T_b, as:

$$T_b = \hat{T}_{b,eq} + T_{b,h}\,\mathrm{sgn}(s) \tag{50}$$

where sgn(s) is the sign function.

The hitting control braking torque, $T_{b,h}$, is determined by the following stability reaching condition (Slotine and Li, 1991):

$$s\dot{s} \le -\eta|s| \tag{51}$$

where $\eta > 0$ is a design parameter. Substituting equation (44) into equation (51) yields:

$$s\left[f - \frac{R_w}{uI_w}(\hat{T}_{b,eq} + T_{b,h}\,\mathrm{sgn}(s)) - a\dot{\lambda}_r\right] \le -\eta|s| \cdot \tag{52}$$

Using the definition for the approximate equivalent control, $\hat{T}_{b,eq}$, as:

$$s(f - \hat{f}) - \frac{R_w}{uI_w} T_{b,h}|s| \le -\eta|s| \cdot \tag{53}$$

Defining the hitting control braking torque, $T_{b,h}$, as:

$$T_{b,h} = \frac{uI_w}{R_w}(F + \eta) \cdot \tag{54}$$

Substituting equation (54) into equation (53) gives:

$$s\dot{s} = |f - \hat{f}||s| - F|s| \le 0 \cdot \tag{55}$$

So that the Lyapunov asymptotic stability condition is satisfied.

The discontinuous switching function, sgn(s), can result in chattering during the sliding motion. Here, the saturation function, sat(□), is used to replace the discontinuous switching function to 'soften' the discontinuity in the control law. Thus, the overall braking torque control, T_b, becomes:

$$T_b = \hat{T}_{b,eq} + T_{b,h}\,sat(s/\Delta) \tag{56}$$

where $\Delta > 0$ is a design parameter, representing the boundary layer thickness. The saturation function is defined as:

$$sat(s/\Delta) = \begin{cases} s/\Delta & |s| < \Delta \\ \mathrm{sgn}(\Delta) & |s| \ge \Delta \end{cases} . \tag{57}$$

3.4. Sliding Mode Sideslip Angle Observer

The sideslip angle must be regulated to improve the

vehicle dynamic performance in the integrated control system, and we have assumed that it can be measurement directly. However, it is very hard to achieve in practice. In this section a sliding mode observer is proposed as a solution to this problem, and the estimated sideslip angle is used in the integrated control system to regulate the motion of the chassis (Hebden *et al.*, 2004).

Under a linear change of coordinates T_o, the nominal state space equation (34) can be expressed in the following form:

$$\dot{X}_1 = A_{11}X_1 + A_{12}X_2 + B_{21}U \tag{58}$$

$$\dot{Y} = \dot{X}_2 = A_{21}X_1 + A_{22}X_2 + B_{22}U + B_{12}f_i \tag{59}$$

where $X_1 = [\Delta\beta \ \Delta\gamma \ \beta]^T$, $Y=X_2=\gamma$. A_{11} has stable eigenvalues. In this new coordinate system, the measurement output noise is included in the unknown but bounded disturbance function f_i. Consider an observer of the form:

$$\dot{\hat{X}}_1 = A_{11}\hat{X}_1 + A_{12}\hat{X}_2 + B_{21}U - A_{12}e_Y \tag{60}$$

$$\dot{\hat{Y}} = A_{21}\hat{X}_1 + A_{22}\hat{X}_2 + B_{22}U - (A_{22} - A_{22}^s)e_Y + v \tag{61}$$

where A_{22}^s is a stable design matrix, and $e_Y=\hat{Y}-Y$. v is a switching term, performed to induce a sliding motion. According to the Lyapunov quadratic stablility conditions, v can be defined as:

$$v = -\rho(t,Y,U)\|B_{12}\|\frac{P_2e_Y}{\|P_2e_Y\|+\Delta} \tag{62}$$

where $\rho(t, Y, U)$ is a scalar function that satisfies:

$$\rho(t,Y,U) > \|f_i\|. \tag{63}$$

P_2 is the unique symmetric positive definition solution to the lyapunov equation:

$$P_2A_{22}^s + A_{22}^{sT}P_2 < 0. \tag{64}$$

Here, the sliding mode observer state space equation (60) and equation (61) can be written as:

$$\dot{\hat{X}} = A_1\hat{X} + B_2U - Le_Y + Hv \tag{65}$$

where the linear gain matrix:

$$L = T_o^{-1}\begin{bmatrix} A_{12} \\ A_{22} - A_{22}^s \end{bmatrix}$$

and the nonlinear gain matrix:

$$H = \|B_{12}\|T_o^{-1}\begin{bmatrix} 0 \\ 1 \end{bmatrix}.$$

By introducing the state estimation error vector $e=\hat{X}-X$, one obtains the following error dynamics:

$$\dot{e} = (A_1 - LC)e + Hv - B_{12}f_i \tag{66}$$

where $C=[0 \ 0 \ 0 \ 1]$.

It is shown in the work of Edwards (1998) that the nonlinear error system in equation (66) is quadratically stable and a sliding motion takes place on the hyper plane $S_o=\{e\in R^n : Ce=0\}$ in finite time.

4. SIMULATION RESULTS

Extensive computer simulations were conducted to evaluate the effectiveness of the sliding mode observer and the integrated control system. The feedback variable sideslip angle used in the control system was observed by the SMO. The observer and the integrated control system were tested under three different critical maneuvers, and the simulation results were compared with that of an FWS vehicle and a DYC only vehicle. The simulation was implemented in the Matlab/Simulink software environment.

4.1. Robustness to Road Condition Variations

In this simulation, the nominal road friction coefficient of the integrated control system is μ=0.8. To examine the robustness of the control system on the low friction coefficient road, a slalom simulation was carried out on a road with friction coefficient μ=0.4. The initial vehicle velocity was set to be 20 m/s. The slalom maneuver is shown in Figure 4a, and was rotated stepwise with increasing step values and increasing time intervals.

Figure 4b is the active front steering angle compensation of the integrated control vehicle. The sideslip angle responses of the FWS vehicle, the only DYC vehicle and the integrated control vehicle are shown in Figure 4c. A comparison of the desired yaw rates and the actual yaw rates of these three vehicles are shown in Figure 4d. We can observe that the FWS vehicle becomes unstable as the steering angle approaches 2 degrees, while the DYC vehicle and the integrated control vehicle can both control their dynamic motions. Nevertheless, compared to the case using only DYC, the yaw rate of the integrated control vehicle can follow the desired yaw rate more exactly, and the sideslip angle can also be regulated more satisfactorily. Figure 4e compares the observed sideslip angle and its actual value. It illustrated that performance of the SMO tracks the actual sideslip angle almost exactly in both magnitude and phase. From Figure 4f and Figure 4g, we can observe that the braking torques of the integrated control vehicle are smaller than those of the only DYC vehicle, and the integrated control vehicle are superior. The simulation result indicates that the integrated control vehicle is less sensitive to the variation of road friction coefficient, and can maintain the steerability and stability more satisfactorily.

4.2. Response to Crosswind Disturbance

The presence of a crosswind can affect the motion of a vehicle at high speed. It can strike and make the vehicle deviate from its course. In this simulation, the road

surface is assumed to be μ=0.8. After running straightly at a constant speed of 35 m/s for 2 seconds, the crosswind is presented. The wind speed is 30 m/s and its yaw angle is 90 degrees. The lateral force disturbance and yaw moment from the crosswind is described in Figure 5a and Figure 5b. From Figure 5d, Figure 5e and Figure 5g, we can observe that the FWS vehicle strays from its course shortly after the crosswind is presented. Compared to that

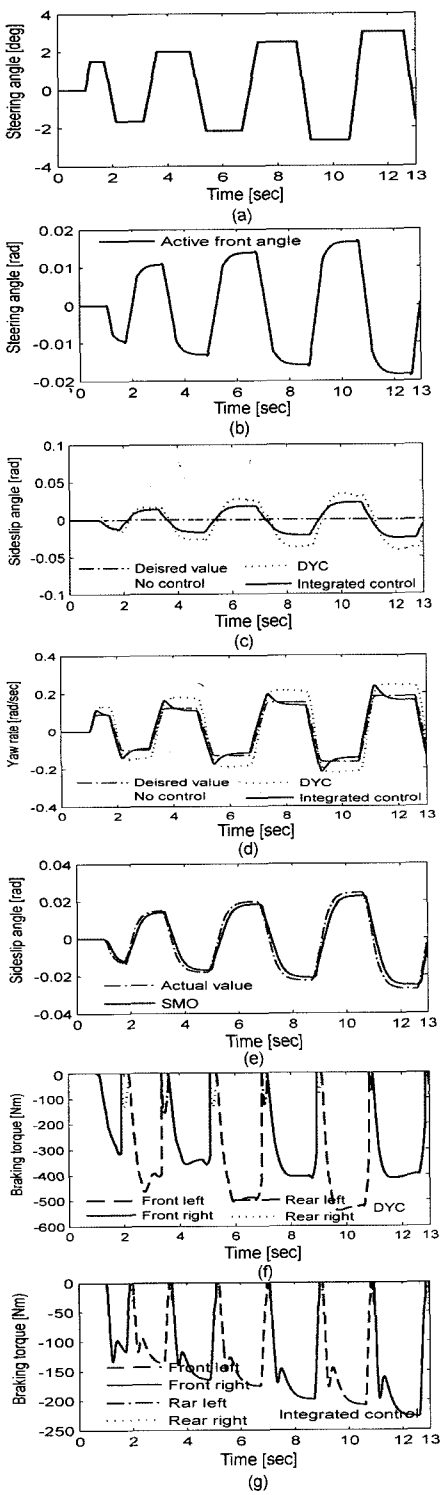

Figure 4. Robustness to road condition variations.

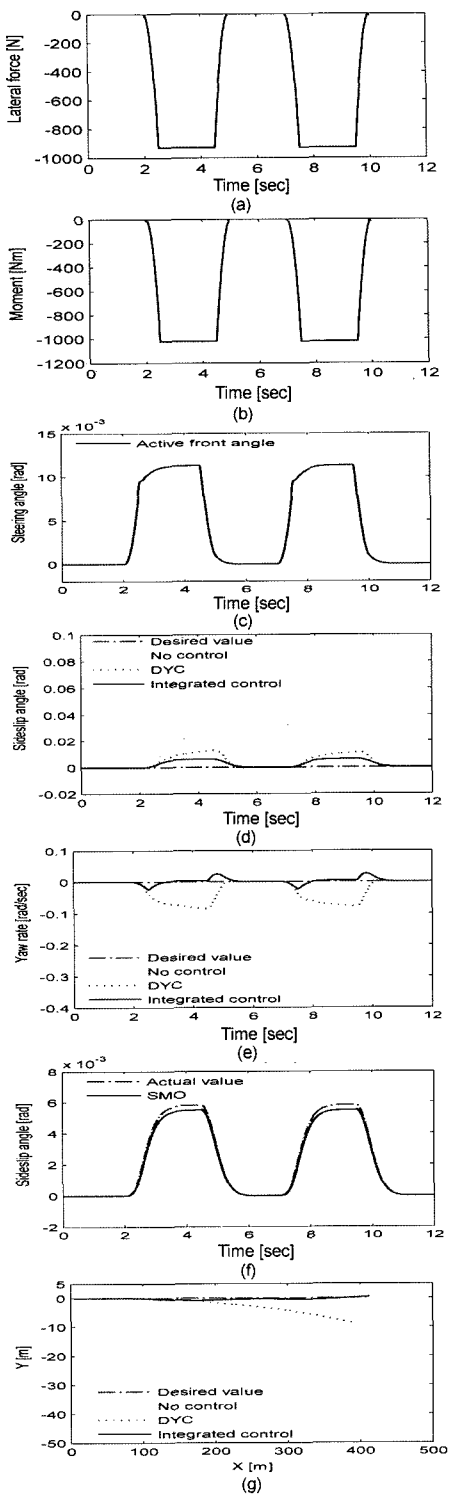

Figure 5. Response to crosswind disturbance.

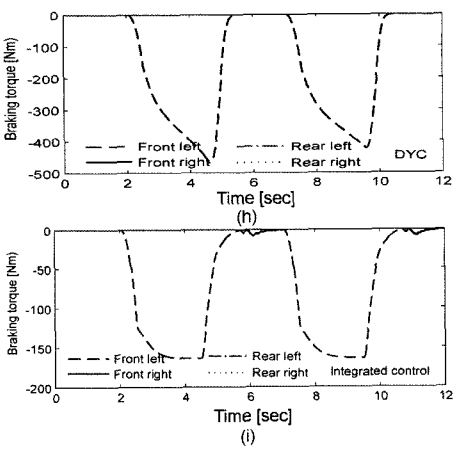

Figure 5. Continued.

of the DYC vehicle, the integrated control vehicle shows satisfactory levels of tracking performance and converging ability to the desired motions. The sideslip angle comparison of the SMO and its actual value of the integrated vehicle are demonstrated in Figure 5f. The effect of the integrated control system on vehicle lateral displacement can be clearly seen from the vehicle trajectories shown in Figure 5g. Figure 5h and Figure 5i show that the front left wheels of the two vehicles have applied braking torques to improve the handling performance, and we can see that the braking torques of the integrated control vehicle is smaller and smoother than that of the DYC only vehicle.

4.3. Braking under μ-Split Conditions

In the case of braking on μ-split maneuver, compatibility between stability and braking performance is impossible by vehicle stabilization control system using only the longitudinal tire forces. The integrated control system can control the front steering angle actively. Then, lateral forces control becomes possible, independently of the longitudinal forces. Therefore, the compatibility is enabled.

The vehicle is initially running straight with a longitudinal velocity of 30 m/s, the desired deceleration is –0.3G for the period of 2s to 4s. The road surface is symmetrical about the central longitudinal axis of the car, with μ=0.8 and μ=0.2 on the right and left sides of the car, respectively. The friction coefficient assumed in the design of the controllers is 0.8 for all tires. Figure 6a is the active front steering angle compensation of the integrated control vehicle. From Figure 6b, Figure 6c, Figure 6d and Figure 6f, we can observe that the FWS vehicle provides large yaw deviation and sideslip angle because of the difference of braking forces between left and right tires. The vehicle starts to yaw and veer to the right side immediately after the simulation begins. The integrated control vehicle can still maintain the deceleration perfor-

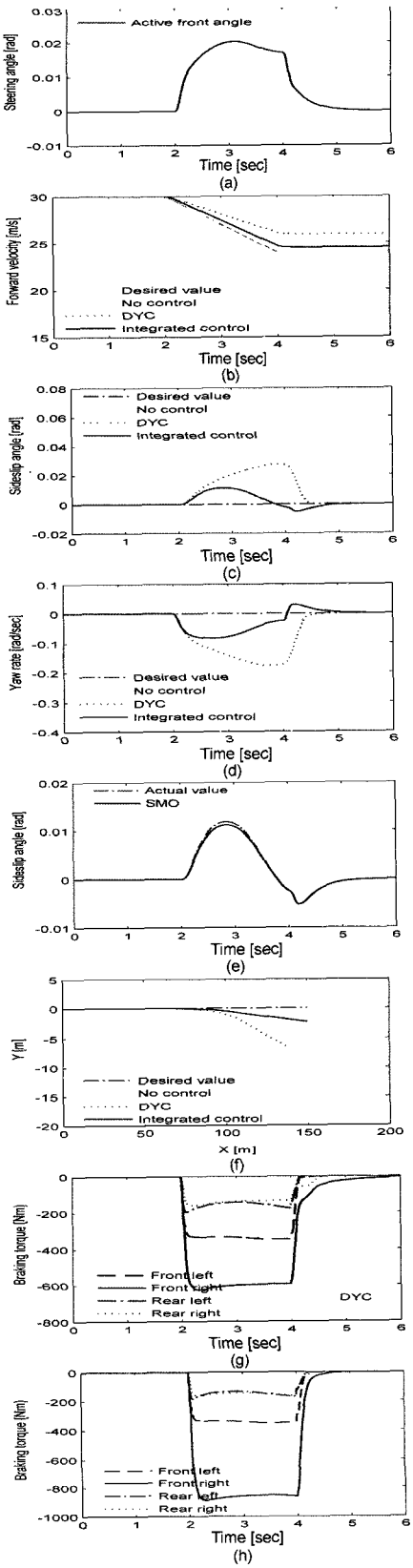

Figure 6. Braking under μ-split conditions.

mance, and regulate the yaw rate and the sideslip angle satisfactorily. On the other hand, even though the yaw rate and sideslip angle can be suppressed, the deceleration performance of the DYC only vehicle deteriorates, as shown in Figure 6b, because the braking torque on the high-μ side must be decreased to equate it to that of the lowest-μ side as possible, which can be seen from Figure 6g and Figure 6h.

5. CONCLUSION

This study proposes a new hierarchical integrated control system of active front wheel steering angle compensation and four wheel braking torque control, based on a sliding sideslip angle mode observer. The performance and robustness of the sliding mode observer and the integrated control system were caused to conform through extensive simulations. The simulation results showed that the sliding mode observer can track the actual sideslip angle satisfactorily in both magnitude and phase, and the integrated control vehicle can follow its desired dynamic motions exactly, even if vehicle parameters change. Compared with the only direct yaw moment control vehicle, the integrated control vehicle exhibits superior handling performance, stability and system robustness under various critical maneuvers.

ACKNOWLEDGEMENT–This work has been supported by the National Development and Reform Commission of China.

REFERENCES

Bartoszewicz, A. (1995). A comment on a time-varying sliding surface for fast and tracking control of second-order dynamic systems. *Automatica* **31**, **12**, 1893–1895.

Boada, B. L., Boada, M. J. L. and Diaz, V. (2005). Fuzzy-logic applied to yaw moment control for vehicle stability. *Vehicle System Dynamics* **43**, **10**, 753–770.

Chun, K. and Sunwoo, M. (2004). Wheel slip control with moving sliding surface for traction control system. *Int. J. Automotive Technology* **5**, **2**, 123–133.

Edwards, C. and Spurgeon, S. K. (1998). *Sliding Mode Control: Theory and Applications.* Taylor & Francis Publications. London.

Gahinet, P., Nemirovski, A., Laub, A. J. and Chilali, M. (1995). *LMI Control Toolbox for Use with MATLAB.* The MathWorks, Inc.

Hebden, R. G., Edwards, C. and Spurgeon, S. K. (2004). Automotive steering control in a split-μ manoeuvre using an observer-based sliding mode controller. *Vehicle System Dynamics* **41**, **3**, 181–202.

Horiuchi, S., Yuhara, N. and Takei, A. (1996). Two degree of freedom/Hinf controller synthesis for active four wheel steering vehicles. *Vehicle System Dynamics* **25**(suppl), 275–292.

Khalil, H. K. (1996). *Nonlinear Systems.* Prentice-Hall. 3th Edn. New Jersey.

Kiencke, U. and Nielsen, L. (2000). *Automotive Control Systems.* Springer-Verlag. Berlin.

Kimbrough, S. (1999). Rule-based wheel slip assignment for vehicle stability enhancement. *SAE Paper No.* 1999-01-0476.

Mokhiamar, Q. and Abe, M. (2002). Wheel steering and yaw moment control combination to maximize stability as well as vehicle responsiveness during quick lane change for active vehicle handling safety. *Proc. Institution of Mechanical Engineers, Part D: J. Automobile Engineering* **216**, **2**, 115–124.

Nagai, M., Nishizawa, Y. and Teranishi, K. (1991). Stability of 4WS vehicle based on side slip zeroing control. Influence of steering system dynamics. *Proc. 6th Int. Pacific Conf. Automotive Engineering,* 951–960.

Nagai, M., Shino, M. and Gao, F. (2002). Study on integrated control of active front steer angle and direct yaw moment. *JSAE Review*, **23**, 309–315.

Nagai, M. and Yamanaka, S. (1996). Integrated control law of active rear wheel steering and direct yaw moment control. *AVEC96*, 451–469.

Nohtomi, S., Okada, K. and Horiuchi, S. (2005). Application of analytic hierarchy process to stochastic robustness synthesis of integrated vehicle controllers. *Vehicle System Dynamics* **42**, **1-2**, 3–21.

Pacejka, H. B. (2002). *Tyre and Vehicle Dynamics.* Butterworth-Heinemann Publications. Oxford.

Qu, Q. Z. and Zu, J. W. (2005). Variable structure model following control of four-wheel-steering vehicle. *Int. J. Vehicle Design* **37**, **4**, 291–310.

Roy, R. G. and Olgac, N. (1997). Robust nonlinear control via moving sliding surfaces-n-th order case. *Proc. 36th IEEE Conf. Decision and Control* 943–948.

Sakai, H. (1990). Study on cornering properties of tire and vehicle. *Tire Science and Technology* **18**, **3**, 136–169.

Shino, M. and Nagai, M. (2001). Yaw-moment control of electric vehicle for improving handling and stability. *JSAE Review* **22**, 473–480.

Skogestad, S. and Postlethwaite, I. (1996). *Multivariable Feedback Control: Analysis and Design.* Wiley Publications. Chichester.

Slotine, J. J. E. and Li, W. (1991). *Applied Nonlinear Control.* Prentice-Hall. New Jersey.

Stéphant, J., Charara, A. and Meizel, D. (2004). Virtual sensor: application to vehicle sideslip angle and transversal forces. *IEEE Trans. Industrial Electronics* **51**, **2**, 278–289.

Suzumura, M., Kojo, T., Tsuchiya, Y. and Asano, K. (2004). Development of the active front steering control system. *AVEC2004*, 53–58.

Zhou, K. and Doyle, J. C. (1997). *Essentials of Robust Control.* Prentice Hall. New Jersey.